The spindle assembly checkpoint and the spatial activation of Polo kinase determine the duration of cell division and prevent neural stem cells tumor formation

Emmanuel Gallaud[1], Laurent Richard-Parpaillon[1], Aude Pascal[1], Mathieu Métivier[1], Vincent Archambault[2] and Régis Giet[1*]

[1] Univ Rennes, CNRS, IGDR (Institut de Génétique et Développement de Rennes) - UMR 6290, F-35000 Rennes, France

[2] Institute for Research in Immunology and Cancer, Université de Montréal, Montréal, QC, Canada.

[*] Corresponding author: regis.giet@univ-rennes1.fr

Abstract

The maintenance of a restricted pool of asymmetrically dividing stem cells is essential for tissue homeostasis. This process requires the control of mitotic progression that ensures the accurate chromosome segregation. In addition, this event is coupled to the asymmetric distribution of cell fate determinants in order to prevent stem cell amplification. How this coupling is regulated remains poorly described. Here, using asymmetrically dividing *Drosophila* neural stem cells (NSCs), we show that Polo kinase activity levels determine the length of cell division, independent of the spindle assembly checkpoint (SAC). This event is mediated by the direct phosphorylation of Polo kinase by Aurora A at spindle poles and Aurora B kinases at centromeres. Furthermore, we show that Aurora A-dependent activation of Polo is the major event that promotes NSC polarization and together with the SAC prevents brain tumor growth. Altogether, our results show that an Aurora/Polo kinase module couples NSC mitotic progression and polarization for tissue homeostasis.

Introduction

The maintenance of a restricted number of stem cells is essential for tissue homeostasis and repair (Daley, 2015). This process has been particularly well described during *Drosophila* brain development; loss of NSCs causes microcephaly while their amplification triggers tissue overgrowth (Caous et al., 2015; Gogendeau et al., 2015; Homem and Knoblich, 2012; Januschke and Gonzalez, 2008; Ramdas Nair et al., 2016). NSCs are subjected to asymmetric cell division. This event is characterized by the asymmetric localization of PAR proteins at the apical cortex that triggers cell fate determinants targeting at the basal cortex. After mitotic spindle alignment along the apico-basal axis, NSC asymmetric cell division gives rise to one cell retaining the NSC proliferation fate while the other cell (GMC for Ganglion Mother Cell) inherits cell fate determinants and is subjected to differentiation (reviewed in (Gallaud et al., 2017)). Both AurA and Polo are needed for cell polarization and for mitotic spindle alignment (Johnston et al., 2009; Lee et al., 2006; Wang et al., 2007, 2006; Wirtz-Peitz et al., 2008). As a consequence, in *aurA* and *polo* mutants, the two daughter cells acquire the NSC proliferative fate, resulting in the amplification of the NSC population and tumor formation in neural tissues. Therefore, in the context of central brain development, *aurA* and *polo* genes are both tumor suppressors (Caous et al., 2015; Lee et al., 2006; Wang et al., 2007, 2006).

Another remarkable feature of *aurA* mutant neural tissue is the absence of obvious chromosome segregations defects despite severe impairment of mitotic spindle assembly (Caous et al., 2015). Correct chromosome segregation in many cell types depends on the Spindle Assembly Checkpoint (SAC) that delays mitotic progression and anaphase onset until all kinetochores are properly attached to spindle microtubules (reviewed in (Corbett, 2017)). As a consequence, ablation of SAC genes in dividing cancer cells induces premature anaphase onset and chromosome segregation defects, cell death or premature differentiation (Caous et al., 2015; Dominguez-Brauer et al., 2015; Gogendeau et al., 2015; Janssen et al., 2009;

Poulton et al., 2017; Silk et al., 2013). *aurA* mutant NSCs show defective mitotic spindle assembly and Cyclin B-Cdk1 levels persist longer than normal, consistent with SAC-dependent mitotic delay (Caous et al., 2015; Giet et al., 2002; Glover et al., 1995). However, SAC ablation in *aurA* mutant does not restore normal mitotic progression, indicating that AurA regulates mitotic progression independently from the SAC (Caous et al., 2015). Altogether, these studies suggest that tissue homeostasis is regulated by AurA kinase that couples mitotic progression to accurate asymmetric cell division of NSCs. The possible AurA targets required for these processes remains elusive. Polo and its human orthologue Plk1 (Polo-like kinase1), were shown, in some cases, to be activated by Aurora kinases *in cellulo* (Bruinsma et al., 2014; Carmena et al., 2012; Joukov et al., 2014; Kachaner et al., 2014; Macůrek et al., 2008; Seki et al., 2008). Polo was therefore a potential candidate to function downstream of Aurora A in NSCs. In this study we analyzed asymmetric cell division and mitotic progression in *polo*, *aurA* and *aurB/Ial* mutants using gain and loss-of function alleles. In the context of the stem-cell based *Drosophila* central brain development, we show here for the first time that asymmetric cell division is coupled to mitotic progression and mainly regulated by the direct activation of Polo kinase by Aurora A and Aurora B *in vivo*.

Result

polo mutants NSCs exhibit a SAC-independent mitotic delay

We first wished to determine if Polo activity promotes mitotic progression in NSCs. To avoid delay caused by possible SAC activation, we examined how time in mitosis was regulated in different *polo* mutants associated with a loss of the SAC gene Mad2 (*polo,mad2*^{P}). Western blotting analyses of brain tissues confirmed the absence of Mad2 in the double mutants and the lower or absent Polo protein levels in weak and strong hypomorphs respectively (Figure 1A). Using live-imaging microscopy, we found that the weak *polo*^{1}/*polo*^{10} and *polo*^{1}/*polo*^{9} hypomorphic mutants showed a prolonged mitosis that was not decreased by absence of the SAC (Figure 1B-C). The time in mitosis was even more prolonged in strong hypomorphic *polo*^{9}/*polo*^{10} mutants but by contrast to weak *polo* hypomorphs, ablation of the SAC decreased the time in mitosis. It indicates a partial SAC contribution to mitotic delay in strong hypomorphic *polo* mutants. This trends were confirmed by analyses of the delay between SAC silencing (as detected by the loss of GFP::Mad2 at kinetochores) and anaphase onset in weak and strong *polo* mutants (Figure 1D-E). As a positive control, NSCs were treated by colchicine to activate the SAC. Under these conditions, GFP::Mad2 signal on the kinetochore persisted during all the duration of the experiment, confirming that the SAC was functional in NSCs (Buffin et al., 2007). The time between SAC silencing and anaphase onset was 0.8 min in controls, 2.1 to 2.4 min in *polo*^{1}/*polo*^{10} and *polo*^{1}/*polo*^{9} and 8.6 min in *polo*^{9}/*polo*^{10} NSCs. This result reveals that weak interference with Polo kinase prolonged mitosis mostly in a SAC-independent manner while mitotic delay is partly SAC-dependent in strong *polo* hypomorphs. Altogether, these results indicate that the SAC cannot account for the prolonged mitosis of weak and strong *polo* hypomorphic mutant NSCs, similarly to *aurA* (Caous et al., 2015).

Thresholds of Polo activation control mitotic progression

In human cultured cells and *Xenopus*, the activation of the Polo orthologue Plk1 was shown to be triggered by the phosphorylation of the conserved Thr210 residue and Plk1 activity is sensitive to Aurora A inhibitors (Bruinsma et al., 2014; Joukov and Nicolo, 2018; Macůrek et al., 2008; Seki et al., 2008). Therefore, we wondered if an Aurora A-mediated activation of Polo kinase could also regulate mitotic progression in NSCs. We hypothesized that the expression of a constitutively active Polo kinase ($Polo^{T182D}$ in flies) should rescue the longer time in mitosis of *aurA* mutants NSCs. In order to test this idea, we generated new transgenic flies allowing the expression of different GFP-tagged variants of Polo kinase in brain tissues including wild-type ($Polo^{WT}$), kinase-dead ($Polo^{K54M}$), constitutively active ($Polo^{T182D}$) and constitutively inactive ($Polo^{T182A}$). Live-imaging experiments on intact brains confirmed that each variant displayed a particular localization on centrosomes, mitotic spindle, midbody and kinetochores of NSCs, similar to what was previously reported in early embryos and S2 cells (Figure S1 and (Kachaner et al., 2017)). Moreover, only $Polo^{WT}$::GFP was able to restore viability of the strong $polo^{9/10}$ hypomorph (hereafter referred to as *polo* mutant) when expressed under the control of a moderate ubiquitous Actin5C promoter (Figure 2A-B). We then assayed the ability of each of these variants to reduce the time in mitosis of *polo* mutant NSCs by live-imaging microscopy (Figure 2C-D). Expression of $Polo^{T182D}$, $Polo^{T182A}$ and $Polo^{K54M}$ in a WT background slightly increased the time in mitosis of NSCs when compared to the expression of $Polo^{WT}$, suggesting hypermorphic or dominant-negative effects. Expression of $Polo^{WT}$ was able to restore a normal time in mitosis when expressed in *polo* mutants. Expression of the $Polo^{T182D}$ variant restored by more than half mitotic duration of *polo* mutant NSCs while expression of the $Polo^{T182A}$ and $Polo^{K54M}$ variants did not. It indicates that Polo kinase activity and more specifically phosphorylation on T182, is required for normal mitotic progression.

We envisaged that the excess of Polo kinase activity caused by expression of Polo^{T182D} in WT and in *polo* mutant cells may be detrimental for spindle assembly and trigger a SAC-dependent mitotic delay (Barbosa et al., 2020; Beck et al., 2013; Foley et al., 2011; Liu et al., 2012; Paschal et al., 2012). We challenged this hypothesis by measuring the time in mitosis of NSCs upon Polo^{T182D} expression in *mad2^{P}* mutant and *polo,mad2^{P}* double mutant (Figure 2E). The moderate increased time in mitosis resulting from Polo^{T182D} expression in WT cells was not abrogated following deletion of the SAC, indicating that this delay did not result from SAC activation but by excess of Polo activity. Congruently, expression of Polo^{T182D} was unable to fully restore the time in mitosis of *polo,mad2^{P}* double mutant NSCs. Altogether, this reveals that a fine-tuning of Polo activity thresholds is crucial to fulfill normal mitotic progression in a SAC-independent manner.

Centrosomal AurA and centromeric Ial/AurB kinases are both required for Polo-dependent mitotic progression

We wanted to investigate if the mitotic progression defect observed in *aurA* and in *aurA,mad2^{P}* mutants shown in our previous study was Polo-kinase-dependent (Caous et al., 2015). Thus, we expressed Polo^{WT} and Polo^{T182D} in these backgrounds (Figure 3A-B and S2A). We found that expression of Polo^{T182D} was able to reduce the time in mitosis of both *aurA* and *aurA,mad2^{P}* mutants NSCs, suggesting that Polo kinase T182 phosphorylation by Aurora A contributes to mitotic progression. In addition, a study have shown that the mitotic phosphorylation of Polo on T182 is also mediated by Aurora B kinase, a component of the Chromosome Passenger Complex (CPC), at centromeres and during cytokinesis (Carmena et al., 2012; Giet and Glover, 2001; Kachaner et al., 2017, 2014). We therefore wondered if the fly orthologue of Aurora B, known as Ial (Ipl1-Aurora-like), was also contributing, with Aurora A, to the control of the time in mitosis through Polo kinase phosphorylation on T182.

As described before for CPC mutants, NSCs from *ial* hypomorphic mutant displayed moderate prolonged mitosis (9.2 min for ial^{2A43}/ial^{1689} vs 6.0 min in a control, Figure 3C-D, S2C and (Mathieu et al., 2013)). This delay was significantly reduced upon $Polo^{T182D}$ expression (8.5 min) indicating that the mitotic delay in *ial* mutant is partially Polo kinase-dependent. Strikingly, combination of *ial* and *aurA* mutations triggered a synergistic delay in the time in mitosis, as most of the double mutant NSCs failed to exit mitosis after 150 min (Figure S2B-C). Polo kinase activity is spatially regulated at the spindle poles and the centromeres by Aurora A and Aurora B respectively ((Joukov and Nicolo, 2018; Magnaghi-Jaulin et al., 2019) for review and (Carmena et al., 2012)). To investigate loss of Aurora kinase activities with spatial activation of Polo, we first monitored the levels of T182 phosphorylation at the centromeres. We found that centromeric Ph-T182 Polo levels were high in control and *aurA* metaphase NSCs and lowered in *polo* and *ial* mutants. We also found that *ial;aurA* double mutants NSCs that were arrested in mitosis displayed nearly normal levels of centromeric Ph-T182 Polo, ruling out that centromeric active Polo is the main contributor that controls mitotic progression (Figure S2D-E). Because the anti- Ph-T182 Polo antibody did not label *Drosophila* mitotic centrosomes, we examined the levels of Centrosomin (Cnn) that oligomerizes and is recruited at centrosomes following direct phosphorylation by Polo kinase (Conduit et al., 2014). The number of cells harboring two Cnn-labeled poles was strongly reduced in *aurA* mutant metaphase cells compared to controls. However, expression of $Polo^{T182D}$ in *aurA* mitotic cells rescued both the number of cells with two Cnn-positive spindle poles but also the amount of protein recruited (Figure S3). Altogether, these results strongly suggest that both Aurora A and Ial phosphorylates Polo on T182 to regulate mitotic progression of NSCs *in vivo*.

Polo and the SAC protect NSCs against aneuploidy and excessive proliferation

Normal brain lobes are characterized by a restricted number of ~100 NSCs (reviewed in (Gallaud et al., 2017)). Defects in cell polarization or spindle orientation trigger the acquisition of a proliferating fate, the amplification of the NSC pool and ultimately tumor formation (Castellanos et al., 2008). Because AurA and Polo are both required for cell polarization and mitotic spindle alignment in NSCs, *aurA* and *polo* mutant brains exhibit higher number of proliferating NSCs and induce tumors when injected in host flies (Caous et al., 2015; Castellanos et al., 2008; Lee et al., 2006; Wang et al., 2007, 2006). To investigate if *polo* mutant-derived tumors share similar characteristics with *aurA* mutant, we undertook a careful analysis of the larval brain tumor derived from *polo* mutants. We found that NSC numbers increased in the central brain of weak *polo* mutants and ablation of the SAC with the $mad2^{P}$ mutation enhanced this amplification (Figure 4A-B). As abnormal NSCs expansion is notoriously abrogated by aneuploidy in flies (Caous et al., 2015; Gogendeau et al., 2015), we monitored the aneuploidy and polyploidy levels of weak *polo* hypomorphs associated with loss of the SAC (Figure 4C-D). We found that aneuploidy and polyploidy level, between 3 and 5% in weak *polo* hypomorphs, was largely increased upon ablation of the SAC (39 to 41%). It indicates that *polo* mutants are prone to segregation errors that are enhanced by loss of the SAC. Altogether, our data show that weak *polo*,$mad2^{P}$ double mutants accumulate chromosome segregation and ploidy defects but exhibit higher NSC amplification. To check if these defects were correlated with changes in tissue proliferation, we performed brain transplantation experiments. We transplanted weak *polo* mutant brain tissues in which the SAC was active or not, in the abdomen of host WT flies and monitored the growth of the transplants (Castellanos et al., 2008; Caussinus and Gonzalez, 2005). Strikingly, inactivation of the SAC and the subsequent increase in aneuploidy correlated with severely enhanced tumor growth of weaker *polo* mutant NSCs (45.1 and 51.5% vs. 22.0 and 24.7% of transplanted flies) (Figure 4E-F). SAC inactivation in a strong *polo* hypomorph background

did not strongly impair NSC number (Figure 4A-B) nor tumor growth (85.2 vs. 86.5% of transplanted flies) (Figure 4E-F). These observations are similar to what was described with *aurA* mutant tumors (Caous et al., 2015). Altogether our data suggest that Polo collaborates with the SAC to protect NSCs against chromosome segregation errors. Moreover, these results also reveal for the first time a case in which tumor growth can be stimulated by aneuploidy in NSCs.

AurA-dependent tumor suppression is mediated by Polo

Polo and AurA both are involved in mitotic progression and act like tumor suppressors in NSCs. Moreover, we noticed that cell size asymmetry resulting from the division of *aurA* mutant NSCs appeared to be rescued by Polo^{T182D} expression (last time point in Figure 3A). Therefore, we decided to investigate if the tumor suppression potential of *aurA* mutants was also Polo-dependent. Consistent with several studies, the NSC number in *aurA* mutants was increased 10 to 25 times compared to control brains (2050 NSCs per lobe, Figure 5A-B) (Caous et al., 2015; Lee et al., 2006; Wang et al., 2006). Strikingly, while expression of Polo^{T182D} had no effect on its own (95 NSCs per lobe), it was sufficient to strongly diminish the NSC amplification incurred in *aurA* mutant tissues (390 NSCs). We also compared tumor growth progression after transplantation of *aurA* mutant neural tissues expressing or not Polo^{T182D} (Figure 5C-D). We found that 90% of transplanted *aurA* mutant brain tissues labeled with mCherry produced large tumors that killed host flies shortly after 15 days. When Polo^{T182D} was expressed in *aurA* mutant, only 10 % and 55 % of the injected hosts developed tumors after 15 and 30 days respectively, indicating that the tumor suppressor potential of AurA is Polo-kinase dependent (Figure 5D). Importantly, the ploidy defects caused by *aurA* mutation (11.8% of the cells) were unchanged following Polo^{T182D} expression (13.1% of the

cells), ruling out differences in ploidy as the cause of the *aurA* mutant tumor growth restriction by Polo^{T182D} (Figure 5E).

At the cellular level, Aurora A is required to regulate larval brain NSC number and growth by controlling mitotic spindle orientation and cell polarization, two characteristics of NSC asymmetric division (Johnston et al., 2009; Lee et al., 2006; Wang et al., 2006; Wirtz-Peitz et al., 2008). We therefore analyzed these two processes in *aurA* mutant NSCs expressing Polo^{T182D}. We first monitored NSC polarization by analyzing the localization of aPKC and Miranda apical and basal crescents respectively. We found that both aPKC and Miranda crescents were properly localized in 100 % of control or Polo^{T182D} expressing NSCs. By contrast and in agreement with previous reports (Lee et al., 2006; Wang et al., 2006), most *aurA* mutant NSCs (78%) displayed homogenous cortical aPKC while Miranda was properly localized at the basal cortex (Figure 5F-H). Strikingly, expression of Polo^{T182D} in *aurA* mutant restored the presence of the aPKC apical crescent in 84% of the NSCs. In parallel, we also measured mitotic spindle alignment along the apico-basal axis in *aurA* mutant with or without Polo^{T182D} expression. In control and Polo^{T182D} expressing NSCs, the vast majority of mitotic spindles were properly oriented in metaphase (angle < 30°: 94% and 100%) while *aurA* mutant NSCs displayed a random mitotic spindle alignment (angle < 30°: 41.8%) in agreement with previous reports (Lee et al., 2006; Wang et al., 2006). We found that Polo^{T182D} expression was sufficient to significantly restore the *aurA* mutant-dependent spindle alignment defects (angle < 30°: 76.3%; Figure 5F, I and J). Altogether, these results indicate that Polo functions downstream of AurA to ensure the asymmetry of NSC divisions to prevent their excessive proliferation during larval brain development.

Discussion

Tissue homeostasis in the fly larval brain requires timely mitotic progression for accurate chromosome segregation. Indeed, chromosome segregation defects trigger the formation aneuploidy NSCs that fail to proliferate (Caous et al., 2015; Gogendeau et al., 2015; Poulton et al., 2017). Mitotic progression is regulated by the maintenance of Cyclin B-CDK1 activity and is under the control of the SAC and a functional APC/C ((Golan et al., 2002; Kraft et al., 2003; Qiao et al., 2016; Zhang et al., 2016) (Corbett, 2017) for review)). In a previous study, we showed that Aurora A kinase was also required for timed and efficient Cyclin B degradation in a SAC-independent manner (Caous et al., 2015). We now bring in this new study details on the molecular mechanism involved: a Aurora-Polo signaling cascade is pivotal to control cell division length. The loss of Aurora A or Ial/Aurora B leads to an extension of the time in mitosis. This mitotic delay can be rescued by the expression of a constitutively active Polo^{T182D}, consistent with the idea that an Aurora-dependent phosphorylation and activation of Polo at T182 is the underlying connection. Our results suggest that although Ial contributes to mitotic progression, the centromeric pool of Polo phosphorylated by Ial does not appear to strongly regulate the time in mitosis because normal levels of Ph-T182 Polo are found in *aurA* mutant and in *ial;aurA* double mutant (Figure S2D-E). By contrast, Cnn recruitment on the centrosomes (as a readout of Polo activity at spindle poles) and mitotic progression are partly rescued in *aurA* mutant following expression of Polo^{T182D} (Figure 3A-B and S3). Altogether, our results suggest that it is mostly centrosomal Aurora A that phosphorylates Polo to regulate Cyclin B degradation and consequently cell division length. The use of weak or strong hypomorphic *polo* mutants and the controlled expression of a dominant Polo^{T182D} active kinase allowed to establish the importance of Polo kinase activity thresholds for mitotic progression. Indeed, weak *polo* hypomorphs are characterized by near normal spindle formation and a prolonged mitosis (~12 min) in which

the SAC has no contribution. Strong *polo* hypomorphs exhibit a longer mitotic delay (~40 min) that is also partly SAC-independent (Figure 1B-C). The use of active Polo^{T182D} allowed highlighting the subversive function of Polo kinase in the control of cell division length. Indeed, when expressed in a wild type or in a strong *polo* mutant background, Polo^{T182D} expression significantly lengthens mitosis even in the absence of the SAC (Figure 2C-E, and (Barbosa et al., 2020)). This reveals that Polo thresholds of activation are essential for timely Cyclin B degradation and mitotic exit *in vivo*. Our observations could therefore explain the apparent antagonism of the literature: Polo inhibits the APC/C activator Cdc20 when the SAC is unsatisfied but is also necessary to phosphorylate and activate APC/C to trigger mitotic exit (Jia et al., 2016; Qiao et al., 2016; Zhang et al., 2016).

Tissue homeostasis depends on the asymmetric distribution of cell fate determinants during NSC division that prevents their excessive proliferation. This process is regulated by tumor suppressor genes ((Gallaud et al., 2017; Homem and Knoblich, 2012; Januschke and Gonzalez, 2008) for review). Strikingly, although Polo and Aurora A were described as tumor suppressors, this work also is the first to demonstrate a direct molecular and functional link between these two kinases in the context of organogenesis. Our study shows that centrosomal Polo phosphorylation by Aurora A governs polarization of neural stem cells but also mitotic spindle orientation, two processes that are essential for appropriate cell fate acquisition during asymmetric cell division ((Gallaud et al., 2017; Homem and Knoblich, 2012; Januschke and Gonzalez, 2008) for review). A past study has proposed that direct phosphorylation of the PAR complex by Aurora A contributes to cell polarization (Wirtz-Peitz et al., 2008). We show here that the amplification of NSCs and the tumor growth of *aurA* mutant brains are strongly inhibited by the expression of an active Polo variant. This restoration of tissue homeostasis is caused by the near complete rescue of cell polarity defects. We therefore suggest that Polo kinase phosphorylation of yet unidentified substrate(s) mediate polarization

of fly NSCs and that the effects of the direct Aurora A phosphorylation of the PAR complex may only play a minor role for Aurora A-dependent tumor suppression. Rescue of spindle orientation in *aurA* mutant by expression of the active Polo^{T182D} may also be mediated by a direct regulation of the spindle orientation machinery by Polo. However, our observations rather favor a model in which this rescue is indirect and stimulated by centrosomal maturation (Figure S3), triggering microtubule nucleation and interactions with the cell cortex ((Conduit et al., 2014; Joukov et al., 2014) and (Magnaghi-Jaulin et al., 2019) for review)). In conclusion, this work has revealed that two essential characteristics of NSCs, the progression of mitosis and cell polarization, are coupled by a signaling cascade leading to the spatial activation of the Polo protein kinase by Aurora kinases. This Aurora/Polo module is critical for tissue development and when impaired, triggers NSC amplification and tumor development. It is also important to emphasize that our study has shown that neural tumors from *polo* mutants seem to have specific characteristics: their progression is aggravated by aneuploidy. Further studies will be required to identify and investigate the functions of the Polo targets in these essential processes and how they are regulated in space and time.

Materials and Methods

Fly strains and alleles combinations

The following strains were used for this study:

UAS-Cherry::Tubulin (BDSC #25774), Ubi-RFP::Tubulin (gift from Renata Basto), UASt-mCherry::Jupiter (gift from Clemens Cabernard), UAS, His2Av::mRFP1 (H2A::RFP, BDSC #23651), His2Av::GFP (H2A::GFP) (Clarkson and Saint, 1999) and GFP::Mad2 (Buffin et al., 2005) were used to monitor by live-imaging the microtubule network, chromosomes and unattached kinetochores. Wild-type (UASp-Polo^{WT}::GFP), phosphomutant (UASp-Polo^{T182A}::GFP), phosphomimic (UASp-Polo^{T182D}::GFP) and kinase-dead (UASp-Polo^{K54M}::GFP) Polo variants tagged with GFP were expressed using the Gal4-UAS system. All four constructs were inserted on the second chromosome (attP40, see below) and on the third chromosome (attP154, (Kachaner et al., 2017)).

Inscuteable-Gal4 (Insc-Gal4; BDSC #8751) and Worniu-Gal4 (Wor-Gal4; BDSC #56554) allowed the expression of UAS driven fluorescent markers in the neuroblasts; and Actin5C-Gal4 (BDSC #4414) was used for ubiquitous expression in somatic cells. The expression of Polo variants for protein level and rescue assays in Figure 2A and 2B as well as the expression of Polo^{T182D}::GFP for ploidy analysis (Figure 5E) were performed using the Actin5C-Gal4 driver. The expression of mCherry::Jupiter and Polo^{T182D}::GFP in *ial* mutant background were driven by Wor-Gal4. For other experiments (live-imaging, immunofluorescence and transplantation assay), Polo variants and the microtubule marker were expressed under the control of Insc-Gal4.

The following alleles were used in this study and described before: *aurA*^{8839} (referred as *aurA* mutant, (Lee et al., 2006; Wang et al., 2006)), *mad2*^{p} (Buffin et al., 2007), *polo*^{1} (Sunkel and Glover, 1988), *polo*^{9} and *polo*^{10} (Donaldson et al., 2001), *ial*^{1689}, *ial*$^{35.33}$ and *ial*^{2A43} (Mathieu et al., 2013). The allelic combination *polo*^{9}/*polo*^{10} (referred as *polo* mutant) corresponds to a

strong *polo* hypomorph mutant and the flies do not reach the pupal stage, as described before (Carmena et al., 2014). The allelic combinations $polo^{1}/polo^{9}$ and $polo^{1}/polo^{10}$ mutant flies are viable and corresponds to weak *polo* hypomorph mutants (Carmena et al., 2014). The phenotype of Ial/Aurora B loss-of-function was assessed during the larval stage using two heteroallelic combinations: $ial^{35.33}/ial^{1689}$ and ial^{2A43}/ial^{1689}.

Flies were maintained and crossed under standard conditions at 25°C.

Generation of transgenes

The constructs containing the coding sequence of Polo variants (WT, T182A, T182D and K54M) C-terminally tagged with GFP were cloned into the plasmid pUAS-K10-attB (Kachaner et al., 2017) and were injected in embryos for targeted insertion on the attP40 site located on second chromosome (BestGene Inc.).

Immunohistochemistry and antibodies

Third instar larval brains (120 to 144 h after egg lying depending on overall growth delay) were dissected in Schneider medium supplemented with 10% FCS and fixed in Testis Buffer (183 mM KCl, 47 mM NaCl, 10 mM Tris, and 1 mM EDTA, pH 6.8) containing 10% formaldehyde and 0.01% Triton X-100 at 25°C for 20 minutes, as described in a previous study (Gallaud et al., 2014).

Primary antibodies: monoclonal anti-α-tubulin DM1A (mouse, 1:500, Sigma T6199), anti-PKCζ (C-20) (rabbit, 1:250, Santa Cruz sc-216), anti-Miranda (rat, 1:200, Abcam 197788), polyclonal anti-phosphorylated Ser10 of Histone H3 (rabbit, 1:500, Millipore 06-570), anti-Deadpan (rat, 1:200, Abcam 195172), anti-Cnn (rabbit, 1:500, (Megraw et al., 1999)) and monoclonal anti-phospho-Plk1T210 (mouse, 1:500, Abcam ab39068).

Secondary antibodies: anti-rat, anti-mouse and anti-rabbit conjugated to 488, 568, 647 Alexa-Fluor (1:500 to 1:1000, Life Technologies).

Images were acquired on a Leica SP5 confocal microscope using 40X (1.25 N.A.) and 63X (1.40 N.A.) objectives, controlled with Leica LAS software and analyzed on Fiji or Imaris.

Western blotting and antibodies

Two to three brains were dissected, resuspended in Laemmli Buffer and loaded on a 4-15% Mini-PROTEAN TGX Precast Protein Gel (BioRad). After migration, proteins are transferred on a nitrocellulose membrane using a Trans-Blot Turbo (BioRad). Membranes were washed with PBS+0.1% Tween20 (PBST) and blocked with PBST+5 to 10% powder milk. The membranes were then incubated in the following primary antibodies, diluted in TBST+2.5 to 5% powder milk: Rabbit polyclonal anti-Actin (I-19, Santa Cruz sc-1616-R; 1/4000), anti-Mad2 (Gift from David Sharp; 1/500), mouse monoclonal anti-Polo MA294 (Gift from David Glover; 1/100). Anti-mouse and anti-Rabbit secondary antibodies were purchased from Jackson ImmunoResearch. Western blots were revealed with SuperSignal West Dura or Femto (ThermoFisher).

Live cell imaging

Third instar larval brains (120 to 144h after egg lying depending on overall growth delay) were dissected in Schneider medium containing 10% FCS and transferred to 50 µL wells (Ibidi, µ-Slide Angiogenesis) for live imaging. Mutant and control brains were imaged in parallel at 25°C. Z-series (thickness of 20 µm with 1 µm spacing) were acquired with a temporal resolution of 30 to 90 s for 1 to 2.5 hours. Alternatively, samples were mounted on a stainless-steel slide, between coverslip and mineral oil as described in a previous study(Gallaud et al., 2014).

Images were acquired with a spinning disk system consisting of a DMi8 microscope (Leica) equipped with a 63X (1.4 N.A.) oil objective, a CSU-X1 spinning disk unit (Yokogawa) and an Evolve EMCCD camera (Photometrics). The microscope was controlled by the Inscoper Imaging Suite and the dedicated software (Inscoper). Alternatively, a CSU-X1 spinning-disk unit mounted on an inverted microscope (Elipse Ti; Nikon) equipped with a 60X (1.4 N.A.) oil objective, a sCMOS ORCA Flash 4.0 (Hamamatsu) and controlled by MetaMorph; was also used for some experiments. Images were processed with Fiji or Imaris softwares.

Image analyses

Time in mitosis

The time in mitosis was determined by the duration between nuclear envelope breakdown NEBD and anaphase onset as described in (Métivier et al., 2020). Note that only the cells undergoing complete mitosis within the span of the experiments were scored. For *ial;aurA* double mutant (Supplementary Figure 2B-C) displaying the most severe phenotype, the cells could not complete mitosis throughout the experiment (2.5 h) and the time in mitosis could not be measured.

Spindle orientation

Spindle orientation on fixed tissue was measured on metaphase cells using the “spot” tool of Imaris. Briefly, two spots were placed in the center of the apical aPKC and basal Miranda crescents to determine the polarity axis; two spots positioned at the spindle poles determined the mitotic spindle axis. For *aurA* mutant that did not exhibit an apical aPKC crescent, the polarity axis was determined by a straight line between the center of the Miranda crescent and a second spot at the opposite cortex. The 3D coordinates of the spots were used to calculate polarity and spindle axes vectors and the angle between them as described in (Loyer and Januschke, 2018).

Cnn intensity

Total intensity was measured on spindle poles of metaphase NSCs using the "spot" tool from Imaris. The spindle poles were defined thanks to the tubulin staining. For each cell, 3 measurements in the cytoplasm were made and the mean of these values was subtracted from the spindle pole intensity values.

Phospho-Plk1 intensity

Z-projections of images restricted to the metaphase plates were made using Fiji ("Sum slices"). Using phospho-Histone H3 staining, metaphase plate shapes were drawn on Fiji (orange lines in Figure S2D) and phospho-Plk1 total signal intensities were measured. Raw intensities were normalized by the volume of measurement.

Ploidy analysis in brains

Third instar larval brains were dissected in PBS, incubated for 8 minutes in 0.5% sodium citrate solution, fixed in acetic acid (45% for 45 seconds and 60% for 2 minutes), squashed between slide and coverslip and flash-frozen in liquid nitrogen (Caous et al., 2015). After coverslip flip off, the squashed cells on the slide were washed in PBS and mounted in ProlonGold supplemented with DAPI. Images were acquired using a Leica DMRXA2 microscope equipped a 63X (1.32 N.A.) objective, a CoolSnap HQ2 camera and controlled by MetaMorph. Images were processed with Fiji software.

Tumor transplantation assay

The protocol to assess proliferation ability of brain tissues was originally set up in the lab of Cayetano Gonzalez (Caussinus and Gonzalez, 2005). Briefly, a central brain fragment (expressing a fluorescent probe) was transplanted in the abdomen of a live wild-type adult female fly and the growth of the transplant was monitored over time. Control or mutant third

instar larval brains, expressing either His2Av::GFP or UAS-Cherry::Tubulin under the control of Insc-Gal4 were dissected in sterile PBS (Sigma). One brain lobe was transplanted in the abdomen of a wild-type adult fly using a pulled capillary with a beveled tip (around 150 µm diameter) adjusted to a microinjection system (IM-9B; Narishige). After transplantation, host flies were maintained at 18°C overnight and transferred at 25°C for a month. Tumor growth was monitored every one or two days upon 30 days for the appearance of a mCherry or GFP signal in the abdomen. For *aurA* and strong *polo* mutants, transplant growth was assessed over a 15-days period because these tumors were particularly aggressive and killed the host flies before 30 days. The neuroblast-specific Insc-Gal4 was used to assay the effect of Polo^{T182D}::GFP variant for tumor growth.

Statistical analyses

Sample size and statistical test used for each analysis are found in the corresponding figure legends. Statistical analyses were performed using the Prism software (Version 7, GraphPad). Three tests were used according to the data. To compare ranks between two unpaired samples with variable variances and non-Gaussian distributions, a nonparametric Mann-Whitney test was used. To compare two unpaired samples with Gaussian distribution, a nonparametric t test was used complemented with a Welch correction if standard deviations were unequal (F test). The comparisons of proportions were assessed by a two-sided Fisher's exact test with a confidence index of 95%. Significance are displayed on the figure: ns: $p>0.05$; *: $p<0.05$; **: $p<0.01$; ***: $p<0.001$; ****: $p<0.0001$.

Acknowledgements:

This work was supported by Fondation pour la Recherche Médicale (DEQ20170336742). We thank members of the "Cytoskeleton and Cell Proliferation" lab, Roland Le Borgne and

Damien Coudreuse for helpful discussions and Laetitia Bataillé for helpful suggestions and critical reading of the manuscript. We are grateful to Renata Basto for advices on tumor growth assays, Clemens Cabernard, David Sharp, Timothy Megraw, Juliette Mathieu and Jean-René Huynh for antibodies, flies and plasmids. We also acknowledge Stéphanie Dutertre and Xavier Pinson for their help using the microscopes of the Microscopy Rennes imaging center facility (MRic).

Author Contributions:

R.G. and E.G. conceived the project. E.G. performed experiments and quantifications with the help of L.R.-P. (Figure 4E-F), A.P. (Figure 2A), R.G. (Figure 1D-E, Figure 4A-D) and M.M. (initial experiment corresponding to Figure 3A-B). R.G. and E.G. discussed the data and wrote the manuscript with the help of V.A.

Competing Interests statement:

The authors declare no competing interests.

Data availability:

Numerical data are available in the Table S1 and all other data are available upon request.

References

Barbosa, J., Martins, T., Bange, T., Tao, L., Conde, C., Sunkel, C., 2020. Polo regulates Spindly to prevent premature stabilization of kinetochore–microtubule attachments. EMBO J. 39. https://doi.org/10.15252/embj.2018100789

Beck, J., Maerki, S., Posch, M., Metzger, T., Persaud, A., Scheel, H., Hofmann, K., Rotin, D., Pedrioli, P., Swedlow, J.R., Peter, M., Sumara, I., 2013. Ubiquitylation-dependent localization of PLK1 in mitosis. Nat. Cell Biol. 15.

Bruinsma, W., Macůrek, L., Freire, R., Lindqvist, A., Medema, R.H., 2014. Bora and Aurora-A continue to activate Plk1 in mitosis. J. Cell Sci. 11.

Buffin, E., Emre, D., Karess, R.E., 2007. Flies without a spindle checkpoint. Nat. Cell Biol. 9, 565–572. https://doi.org/10.1038/ncb1570

Buffin, E., Lefebvre, C., Huang, J., Gagou, M.E., Karess, R.E., 2005. Recruitment of Mad2 to the Kinetochore Requires the Rod/Zw10 Complex. Curr. Biol. 15, 856–861. https://doi.org/10.1016/j.cub.2005.03.052

Caous, R., Pascal, A., Romé, P., Richard-Parpaillon, L., Karess, R.E., Giet, R., 2015. Spindle assembly checkpoint inactivation fails to suppress neuroblast tumour formation in aurA mutant Drosophila. Nat. Commun. 6.

Carmena, M., Lombardia, M.O., Ogawa, H., Earnshaw, W.C., 2014. Polo kinase regulates the localization and activity of the chromosomal passenger complex in meiosis and mitosis in *Drosophila melanogaster*. Open Biol. 4, 140162. https://doi.org/10.1098/rsob.140162

Carmena, M., Pinson, X., Platani, M., Salloum, Z., Xu, Z., Clark, A., Ogawa, H., Eggert, U., Glover, D.M., Archambault, V., 2012. The Chromosomal Passenger Complex Activates Polo Kinase at Centromeres. PLoS Biol. 10, 15.

Castellanos, E., Dominguez, P., Gonzalez, C., 2008. Centrosome Dysfunction in Drosophila Neural Stem Cells Causes Tumors that Are Not Due to Genome Instability. Curr. Biol. 18, 1209–1214. https://doi.org/10.1016/j.cub.2008.07.029

Caussinus, E., Gonzalez, C., 2005. Induction of tumor growth by altered stem-cell asymmetric division in Drosophila melanogaster. Nat. Genet. 37, 1125–1129. https://doi.org/10.1038/ng1632

Clarkson, M., Saint, R., 1999. A His2AvDGFP Fusion Gene Complements a Lethal His2AvD Mutant Allele and Provides an in Vivo Marker for Drosophila Chromosome Behavior. DNA Cell Biol. 18, 457–462. https://doi.org/10.1089/104454999315178

Conduit, P.T., Feng, Z., Richens, J.H., Baumbach, J., Wainman, A., Bakshi, S.D., Dobbelaere, J., Johnson, S., Lea, S.M., Raff, J.W., 2014. The Centrosome-Specific Phosphorylation of Cnn by Polo/Plk1 Drives Cnn Scaffold Assembly and Centrosome Maturation. Dev. Cell 28, 659–669. https://doi.org/10.1016/j.devcel.2014.02.013

Corbett, K.D., 2017. Molecular Mechanisms of Spindle Assembly Checkpoint Activation and Silencing, in: Black, B.E. (Ed.), Centromeres and Kinetochores, Progress in Molecular and Subcellular Biology. Springer International Publishing, Cham, pp. 429–455. https://doi.org/10.1007/978-3-319-58592-5_18

Daley, G.Q., 2015. Stem cells and the evolving notion of cellular identity. Philos. Trans. R. Soc. B Biol. Sci. 370, 5.

Dominguez-Brauer, C., Thu, K.L., Mason, J.M., Blaser, H., Bray, M.R., Mak, T.W., 2015.

Targeting Mitosis in Cancer: Emerging Strategies. Mol. Cell 60, 524–536. https://doi.org/10.1016/j.molcel.2015.11.006

Donaldson, M.M., Tavares, Á.A.M., Ohkura, H., Deak, P., Glover, D.M., 2001. Metaphase Arrest with Centromere Separation in polo Mutants of Drosophila. J. Cell Biol. 153, 663–676. https://doi.org/10.1083/jcb.153.4.663

Foley, E.A., Maldonado, M., Kapoor, T.M., 2011. Formation of stable attachments between kinetochores and microtubules depends on the B56-PP2A phosphatase. Nat. Cell Biol. 13.

Gallaud, E., Caous, R., Pascal, A., Bazile, F., Gagné, J.-P., Huet, S., Poirier, G.G., Chrétien, D., Richard-Parpaillon, L., Giet, R., 2014. Ensconsin/Map7 promotes microtubule growth and centrosome separation in Drosophila neural stem cells. J. Cell Biol. 204, 1111–1121. https://doi.org/10.1083/jcb.201311094

Gallaud, E., Pham, T., Cabernard, C., 2017. Drosophila melanogaster Neuroblasts: A Model for Asymmetric Stem Cell Divisions, in: Tassan, J.-P., Kubiak, J.Z. (Eds.), Asymmetric Cell Division in Development, Differentiation and Cancer, Results and Problems in Cell Differentiation. Springer International Publishing, Cham, pp. 183–210. https://doi.org/10.1007/978-3-319-53150-2_8

Giet, R., Glover, D.M., 2001. Drosophila Aurora B Kinase Is Required for Histone H3 Phosphorylation and Condensin Recruitment during Chromosome Condensation and to Organize the Central Spindle during Cytokinesis. J. Cell Biol. 152, 669–682. https://doi.org/10.1083/jcb.152.4.669

Giet, R., McLean, D., Descamps, S., Lee, M.J., Raff, J.W., Prigent, C., Glover, D.M., 2002. Drosophila Aurora A kinase is required to localize D-TACC to centrosomes and to regulate astral microtubules. J. Cell Biol. 156, 437–451. https://doi.org/10.1083/jcb.200108135

Glover, D.M., Leibowitz, M.H., McLean, D.A., Parry, H., 1995. Mutations in aurora prevent centrosome separation leading to the formation of monopolar spindles. Cell 81, 95–105. https://doi.org/10.1016/0092-8674(95)90374-7

Gogendeau, D., Siudeja, K., Gambarotto, D., Pennetier, C., Bardin, A.J., Basto, R., 2015. Aneuploidy causes premature differentiation of neural and intestinal stem cells. Nat. Commun. 6, 8894. https://doi.org/10.1038/ncomms9894

Golan, A., Yudkovsky, Y., Hershko, A., 2002. The Cyclin-Ubiquitin Ligase Activity of Cyclosome/APC Is Jointly Activated by Protein Kinases Cdk1-Cyclin B and Plk. J. Biol. Chem. 277.

Homem, C.C.F., Knoblich, J.A., 2012. Drosophila neuroblasts: a model for stem cell biology. Development 139, 4297–4310. https://doi.org/10.1242/dev.080515

Janssen, A., Kops, G.J.P.L., Medema, R.H., 2009. Elevating the frequency of chromosome mis-segregation as a strategy to kill tumor cells. Proc. Natl. Acad. Sci. 106, 19108–19113. https://doi.org/10.1073/pnas.0904343106

Januschke, J., Gonzalez, C., 2008. Drosophila asymmetric division, polarity and cancer. Oncogene 27, 6994–7002. https://doi.org/10.1038/onc.2008.349

Jia, L., Li, B., Yu, H., 2016. The Bub1–Plk1 kinase complex promotes spindle checkpoint signalling through Cdc20 phosphorylation. Nat. Commun. 7, 10818. https://doi.org/10.1038/ncomms10818

Johnston, C.A., Hirono, K., Prehoda, K.E., Doe, C.Q., 2009. Identification of an Aurora-A/PinsLINKER/ Dlg Spindle Orientation Pathway using Induced Cell Polarity in S2 Cells.

Cell 138, 1150–1163. https://doi.org/10.1016/j.cell.2009.07.041

Joukov, V., Nicolo, A.D., 2018. Aurora-PLK1 cascades as key signaling modules in the regulation of mitosis. Sci. Signal. 26.

Joukov, V., Walter, J.C., De Nicolo, A., 2014. The Cep192-Organized Aurora A-Plk1 Cascade Is Essential for Centrosome Cycle and Bipolar Spindle Assembly. Mol. Cell 55, 578–591. https://doi.org/10.1016/j.molcel.2014.06.016

Kachaner, D., Garrido, D., Mehsen, H., Normandin, K., Lavoie, H., Archambault, V., 2017. Coupling of Polo kinase activation to nuclear localization by a bifunctional NLS is required during mitotic entry. Nat. Commun. 8.

Kachaner, D., Pinson, X., El Kadhi, K.B., Normandin, K., Talje, L., Lavoie, H., Lépine, G., Carréno, S., Kwok, B.H., Hickson, G.R., Archambault, V., 2014. Interdomain allosteric regulation of Polo kinase by Aurora B and Map205 is required for cytokinesis. J. Cell Biol. 207, 201–211. https://doi.org/10.1083/jcb.201408081

Kraft, C., Herzog, F., Gieffers, C., Mechtler, K., Hagting, A., Pines, J., Peters, J.-M., 2003. Mitotic regulation of the human anaphase-promoting complex by phosphorylation. EMBO J. 22, 6598–6609. https://doi.org/10.1093/emboj/cdg627

Lee, C.-Y., Andersen, R.O., Cabernard, C., Manning, L., Tran, K.D., Lanskey, M.J., Bashirullah, A., Doe, C.Q., 2006. Drosophila Aurora-A kinase inhibits neuroblast self-renewal by regulating aPKC/Numb cortical polarity and spindle orientation. Genes Dev. 20, 3464–3474. https://doi.org/10.1101/gad.1489406

Liu, D., Davydenko, O., Lampson, M.A., 2012. Polo-like kinase-1 regulates kinetochore–microtubule dynamics and spindle checkpoint silencing. J. Cell Biol. 198, 491–499. https://doi.org/10.1083/jcb.201205090

Loyer, N., Januschke, J., 2018. The last-born daughter cell contributes to division orientation of Drosophila larval neuroblasts. Nat. Commun. 9, 12.

Macůrek, L., Lindqvist, A., Lim, D., Lampson, M.A., Klompmaker, R., Freire, R., Clouin, C., Taylor, S.S., Yaffe, M.B., Medema, R.H., 2008. Polo-like kinase-1 is activated by aurora A to promote checkpoint recovery. Nature 455, 119–123. https://doi.org/10.1038/nature07185

Magnaghi-Jaulin, L., Eot-Houllier, G., Gallaud, E., Giet, R., 2019. Aurora A Protein Kinase: To the Centrosome and Beyond. Biomolecules 9, 28. https://doi.org/10.3390/biom9010028

Mathieu, J., Cauvin, C., Moch, C., Radford, S.J., Sampaio, P., Perdigoto, C.N., Schweisguth, F., Bardin, A.J., Sunkel, C.E., McKim, K., Echard, A., Huynh, J.-R., 2013. Aurora B and Cyclin B Have Opposite Effects on the Timing of Cytokinesis Abscission in Drosophila Germ Cells and in Vertebrate Somatic Cells. Dev. Cell 26, 250–265. https://doi.org/10.1016/j.devcel.2013.07.005

Megraw, T.L., Li, K., Kao, L.-R., Kaufman, T.C., 1999. The Centrosomin protein is required for centrosome assembly and function during cleavage in Drosophila. Development 126, 2829–2839.

Métivier, M., Gallaud, E., Thomas, A., Pascal, A., Gagné, J.-P., Poirier, G.G., Chrétien, D., Gibeaux, R., Richard-Parpaillon, L., Benaud, C., Giet, R., 2020. Drosophila Tubulin-Specific Chaperone E Recruits Tubulin around Chromatin to Promote Mitotic Spindle Assembly. Curr. Biol. S0960982220316845. https://doi.org/10.1016/j.cub.2020.11.009

Paschal, C.R., Maciejowski, J., Jallepalli, P.V., 2012. A stringent requirement for Plk1 T210 phosphorylation during K-fiber assembly and chromosome congression. Chromosoma 121.

Poulton, J.S., Cuningham, J.C., Peifer, M., 2017. Centrosome and spindle assembly checkpoint loss leads to neural apoptosis and reduced brain size. J. Cell Biol. 216, 11.

Qiao, R., Weissmann, F., Yamaguchi, M., Brown, N.G., VanderLinden, R., Imre, R., Jarvis, M.A., Brunner, M.R., Davidson, I.F., Litos, G., Haselbach, D., Mechtler, K., Stark, H., Schulman, B.A., Peters, J.-M., 2016. Mechanism of APC/CCDC20 activation by mitotic phosphorylation. Proc. Natl. Acad. Sci. 113, 9.

Ramdas Nair, A., Singh, P., Salvador Garcia, D., Rodriguez-Crespo, D., Egger, B., Cabernard, C., 2016. The Microcephaly-Associated Protein Wdr62/CG7337 Is Required to Maintain Centrosome Asymmetry in Drosophila Neuroblasts. Cell Rep. 14, 1100–1113. https://doi.org/10.1016/j.celrep.2015.12.097

Seki, A., Coppinger, J.A., Jang, C.-Y., Iii, J.R.Y., Fang, G., 2008. Bora and the Kinase Aurora A Cooperatively Activate the Kinase Plk1 and Control Mitotic Entry. Science 320, 5.

Silk, A.D., Zasadil, L.M., Holland, A.J., Vitre, B., Cleveland, D.W., Weaver, B.A., 2013. Chromosome missegregation rate predicts whether aneuploidy will promote or suppress tumors. Proc. Natl. Acad. Sci. 110, E4134–E4141. https://doi.org/10.1073/pnas.1317042110

Sunkel, C.E., Glover, D.M., 1988. polo, a mitotic mutant of Drosophila displaying abnormal spindle poles. J. Cell Sci. 89.

Wang, H., Ouyang, Y., Somers, W.G., Chia, W., Lu, B., 2007. Polo inhibits progenitor self-renewal and regulates Numb asymmetry by phosphorylating Pon. Nature 449, 96–100. https://doi.org/10.1038/nature06056

Wang, H., Somers, G.W., Bashirullah, A., Heberlein, U., Yu, F., Chia, W., 2006. Aurora-A acts as a tumor suppressor and regulates self-renewal of Drosophila neuroblasts. Genes Dev. 20, 3453–3463. https://doi.org/10.1101/gad.1487506

Wirtz-Peitz, F., Nishimura, T., Knoblich, J.A., 2008. Linking Cell Cycle to Asymmetric Division: Aurora-A Phosphorylates the Par Complex to Regulate Numb Localization. Cell 135, 161–173. https://doi.org/10.1016/j.cell.2008.07.049

Zhang, S., Chang, L., Alfieri, C., Zhang, Z., Yang, J., Maslen, S., Skehel, M., Barford, D., 2016. Molecular mechanism of APC/C activation by mitotic phosphorylation. Nature 533, 19.

Figure legends

Figure 1: *polo* mutant NSCs display a SAC-independent mitotic delay.

A) Polo, Mad2 and Actin Western blot analyses in *polo* and *polo,mad2*^{P} mutant brain extracts. The genotypes are indicated for each lane. *polo*^{1}/*polo*^{10} and *polo*^{1}/*polo*^{9} are weak hypomorphs and *polo*^{9}/*polo*^{10} is a strong hypomorph. **B)** Time-lapse imaging of mitosis in *polo* mutants in the absence or presence of Mad2. Selected image series of dividing NSCs of the indicated genotypes expressing mCherry::Tubulin (from top to bottom). The white dashed line outlines the dividing NSCs. Scale bar: 5 µm. Time is min:s (t=00:00 is NEBD). **C)** Quantification of time in mitosis from NEBD to anaphase onset for NSCs of the indicated genotypes. Means are shown as black bars. Mann-Whitney unpaired test: ns: $p>0.05$; *: $p<0.05$; ****: $p<0.0001$. **D)** GFP::Mad2 kinetochore localization in control, colchicine-treated, and *polo* mutant NSCs expressing H2A::RFP. Colchicine treatment (20µM) was used as a control for GFP::Mad2 accumulation on kinetochores. Yellow arrowheads indicate the last kinetochore labeled with GFP::Mad2 before anaphase onset (AO). Scale bar: 5 µm. Time is min:s (t=00:00 is the beginning of the experiment). **E)** Quantification of the time between SAC satisfaction (disappearance of the last GFP::Mad2-labeled kinetochores) and anaphase onset in NSCs of the indicated genotypes. Means are shown as black bars. Mann-Whitney unpaired test: ****: $p<0.0001$. Numerical data (mean, SD and *n*) related to all the figures are available in Table S1.

Figure 2: Loss or excess of Polo activity is not compatible with normal mitosis duration and *Drosophila* viability.

A) Polo and Actin Western blot analyses showing the expression of endogenous Polo kinase in control and GFP-tagged Polo variants (WT, T182D, T182A and K54M) expressed ubiquitously in *polo* mutant brains. The genotypes are indicated for each lane. Actin was used

as a loading control. **B)** Hatching rates of *polo* mutants expressing the indicated Polo variants. **C)** Time-lapse imaging of mitosis in *polo* mutant NSCs expressing the indicated Polo variants and mCherry::Tubulin. The white dashed lines outline the dividing NSCs. Scale bar: 5 µm. Time is min:s (t=00:00 is NEBD). **D-E)** Quantification of the time in mitosis of NSCs of the indicated genotypes. Means are shown as black bars. Mann-Whitney unpaired test: ns: p>0.05; *: $p<0.05$; ****: $p<0.0001$.

Figure 3: Mitotic delays in *aurA* and *aurB* mutants are Polo-dependent.

A, C) Time-lapse imaging of mitosis in *aurA* and *aurB/ial* mutant NSCs expressing the indicated Polo variants and mCherry::Tubulin. The white dashed lines outline the dividing NSCs. Scale bar: 5 µm. Time is min:s (t=00:00 is NEBD). **B, D)** Quantification of time in mitosis for the indicated genotypes. Means are shown as black bars. Mann-Whitney unpaired tests: ns: $p>0.05$; *: $p<0.05$; **: $p<0.01$; ****: $p<0.0001$.

Figure 4: Impairing the SAC in *polo* mutants induces aneuploidy and promotes tumor growth.

A) Representative images of larval brain lobes of the indicated genotypes stained for the NSC marker Deadpan. The white dashed lines outline the central brain area where NSCs were scored. Note the reduced brain lobe size in the $polo^{9/10}$ mutant. Scale bar: 100 µm. **B)** Quantifications of Deadpan-positive NSCs per brain lobe for the indicated genotypes. Mann-Whitney unpaired test: *: $p<0.05$; ****: $p<0.0001$. Means are shown in black. **C)** Representative images of the three classes of mitotic figures observed from squashed brains stained with DAPI: euploid (8 chromosomes), aneuploid (more or less than 8 chromosomes) and polyploid (multiple of 8 chromosomes) cells. Scale bar: 10 µm. **D)** Percentage of mitotic brain cells with ploidy defects (aneuploidy and polyploidy) for the indicated genotypes. For

statistical analyses, the proportion of euploidy was compared to the proportion of ploidy defects. Fisher's exact test: ns: $p>0.05$; *: $p<0.05$; ****: $p<0.0001$. **E)** Examples of wild-type adult host flies 30 and 15 days after transplantation with control and *polo* mutant brain lobe expressing H2A::GFP as a readout for tumor development (bottom). Asterisks indicate transplantation scars. **F)** Proportion of host flies developing tumors following the transplantation of brain lobes from the indicated genotypes. Fisher's exact test; ns: $p>0.05$; *: $p<0.05$; ***: $p<0.001$.

Figure 5: Activation of Polo restores NSCs polarization, spindle orientation and inhibits tumor growth in an *aurA* mutant.

A) Representative images of fixed control and *aurA* mutant larval brain lobes with or without $Polo^{T182D}$::GFP expression and stained for the NSC marker Deadpan. The white dashed lines outline the central brain area where NSCs were scored. Note that the expression $Polo^{T182D}$ in *aurA* mutant restores the delimitation between the central brain and neuroepithelium. Scale bar: 100 µm. **B)** Quantification of the NSC number in each brain lobe for the indicated genotypes. **C)** Examples of wild-type adult host flies 15 and 30 days after transplantation with *aurA* mutant or *aurA* mutant expressing $Polo^{T182D}$::GFP brain lobes expressing mCherry::Tubulin as a readout to follow tumor development. Red asterisks indicate transplantation scars. **D)** Percentage of host flies developing tumors 15 and 30 days after the transplantation of brain lobes from the indicated genotypes. **E)** Quantification of ploidy defects scored in neural tissue for the indicated genotypes. The proportion of euploidy was compared to the proportion of ploidy defects for statistical analyses. **F)** Representative images of control, $Polo^{T182D}$::GFP, *aurA* mutant and $Polo^{T182D}$::GFP;*aurA* metaphase NSCs stained for Miranda (magenta in the merge), aPKC and Phospho-Histone H3 (green in the merge), and α-Tubulin (white in the merge). Yellow arrowheads indicate the edges of aPKC crescent.

Scale bar: 5 µm. **G)** Schematic representation of aPKC localization patterns observed in NSCs: left: aPKC forms a crescent which defines the apical cortex of the control cell; right: aPKC is unpolarized and exhibits an homogenous cytoplasmic and cortical localization. **H)** Percentage of NSCs of the indicated genotypes with either a polarized apical crescent (light grey) or homogenous cortical and cytoplasmic aPKC localization (dark grey). **I)** Schematic illustration of the method used to measure the spindle alignment α angle (orange) between the polarity axis (black dashed line), determined by aPKC (green) and Miranda (magenta), and the spindle axis (blue dashed line) determined by spindle poles (See Methods). **J)** Quantification of the α angle between polarity and spindle axes in metaphase NSCs for the indicated genotypes. Mann-Whitney unpaired test: ns: $p>0.05$; ****: $p<0.0001$. Means are shown as black bars. For panels D), E) and H): Fisher's exact test: ns: $p>0.05$; *: $p<0.05$, ***: $p<0.001$; ****: $p<0.0001$.

Supplementary Figure S1: Localization of GFP-tagged Polo variants during NSC division.

A) Time-lapse imaging of cell division in NSCs expressing the indicated Polo variants and mCherry::Tubulin. The white dashed line outlines the NSCs. Scale bar: 5 µm. Time is min:s (t=00:00 is NEBD). **B)** Summary table of Polo variants localization patterns along cell cycle stages. The symbols "-", "+/-", "+" and "++" reflect absence, variable localization, moderate localization and strong enrichment, respectively.

Supplementary Figure S2: Time in mitosis analyses in Polo^{T182D}::GFP;*aurA,mad2^{P}* and *ial;aurA* mutant NSCs.

A) Quantification of the time in mitosis for the indicated genotypes. **B)** Time-lapse imaging of dividing NSCs for control and *ial;aurA* double mutant NSCs expressing RFP::Tubulin. The

white dashed lines outline the dividing NSCs. Scale bar: 5 µm. Time is h:min:s (t=0:00:00 is the beginning of the experiment). **C)** Quantification of the time in mitosis of NSCs of the indicated genotypes. The *ial;aurA* double mutant NSCs displayed a severe mitotic delay that could not be quantified since the vast majority did not exit mitosis during the duration of the experiment (2.5 hours). Mann-Whitney unpaired test: ns: $p>0.05$; ****: $p<0.0001$. **D)** Representative images of metaphase NSCs of the indicated genotypes stained for phospho-Plk1 (white in the merge), aPKC and Phospho-Histone H3 (magenta in the merge) and tubulin (green in the merge). The orange shapes in the right column outline the metaphase plates, according to the Phospho-Histone H3-labeled metaphase plate, in which phospho-Plk1 signal was measured. Scale bar: 5 µm. **E)** Quantification of phospho-Plk1 signal for the indicated genotypes, normalized by the area of measurement. Unpaired t-test: ns: $p>0.05$; **: $p<0.01$; ***: $p<0.001$; ****: $p<0.0001$.

Supplementary Figure S3: Polo activation restores centrosome maturation in *aurA* mutant NSCs

A) Representative images of metaphase NSCs of the indicated genotypes stained for Miranda (magenta in the merge), aPKC and Cnn (green in the merge) and tubulin (white in the merge). The yellow arrowheads in the bottom line highlight the Cnn-labeled spindle poles. Scale bar: 5 µm. **B)** Percentage of metaphase NSCs displaying two, one or no Cnn-labeled centrosomes per cell for the indicated genotypes. Fisher's exact test: ns: $p>0.05$; ****: $p<0.0001$. **C)** Quantification of normalized Cnn intensity at spindle poles for the indicated genotypes. Mann-Whitney unpaired tests: ns: $p>0.05$; **: $p<0.01$; ****: $p<0.0001$.

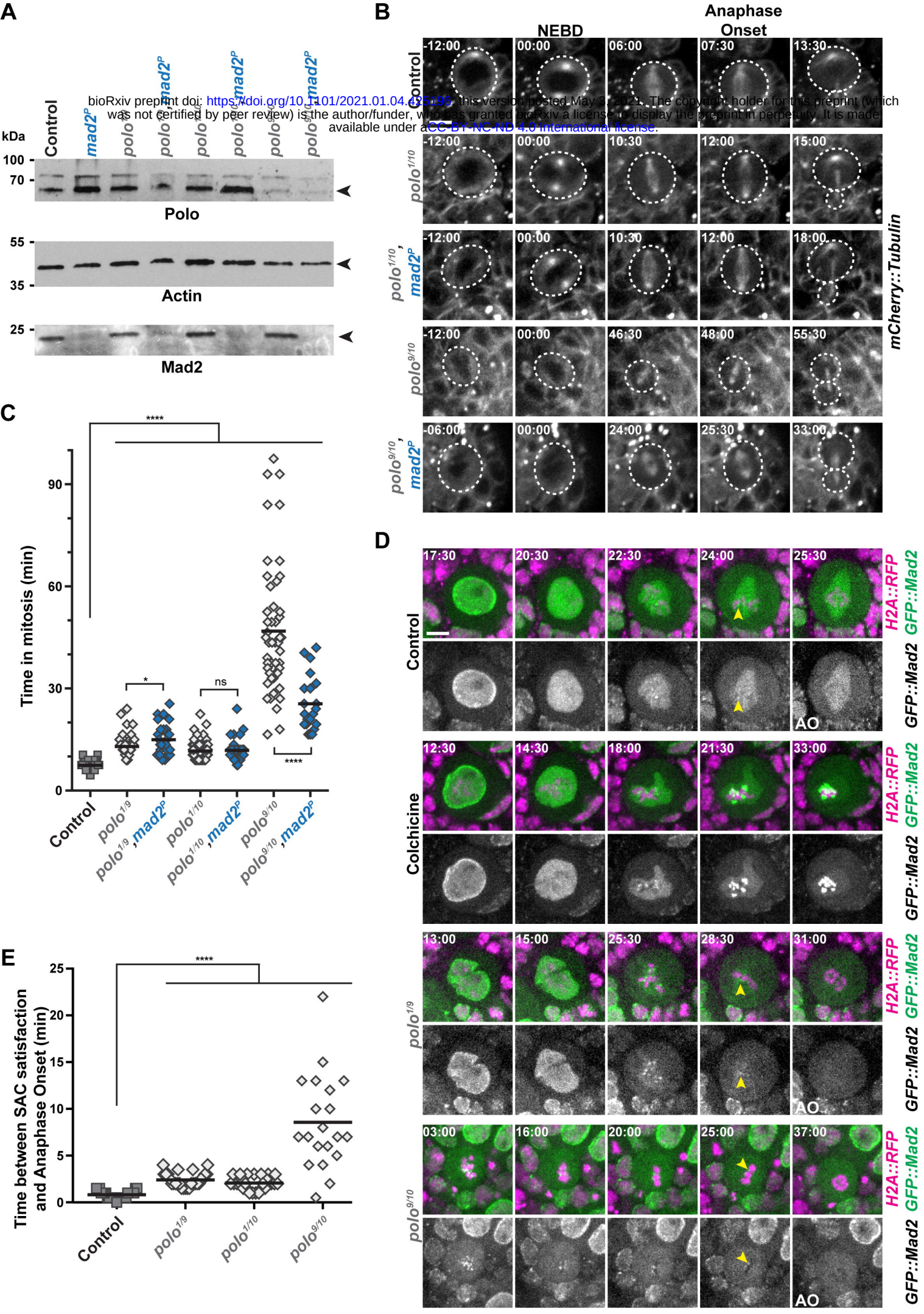

Figure 1

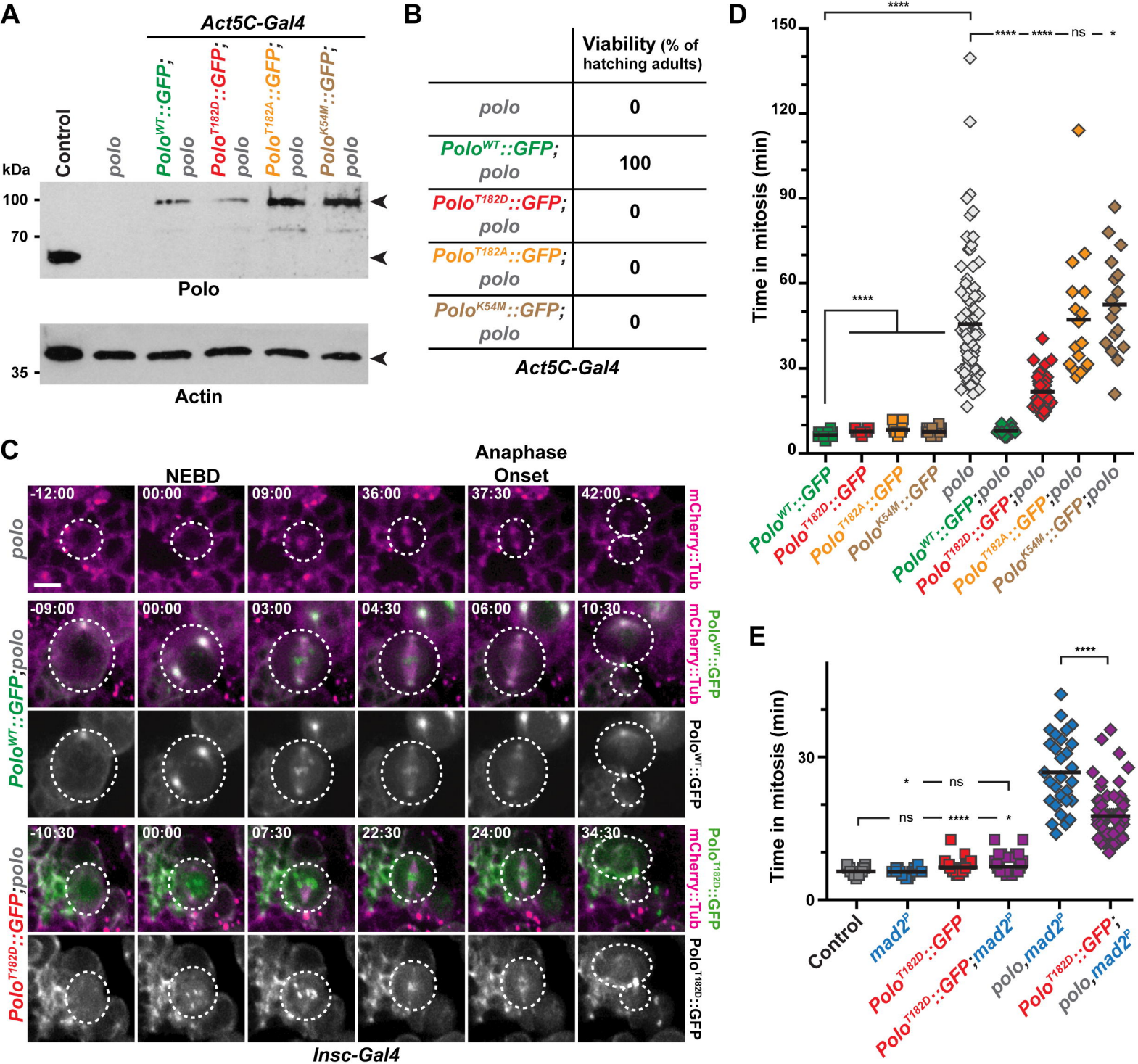
A
Act5C-Gal4
Control
polo
Polo^WT::GFP; polo
Polo^T182D::GFP; polo
Polo^T182A::GFP; polo
Polo^K54M::GFP; polo
kDa
100
70
35
Polo
Actin
B
Viability (% of hatching adults)
polo 0
Polo^WT::GFP; polo 100
Polo^T182D::GFP; polo 0
Polo^T182A::GFP; polo 0
Polo^K54M::GFP; polo 0
Act5C-Gal4
C
NEBD
Anaphase Onset
polo
Polo^WT::GFP;polo
Polo^T182D::GFP;polo
mCherry::Tub
Polo^WT::GFP
Polo^T182D::GFP
Insc-Gal4
D
Time in mitosis (min)
150
120
90
60
30
0
****
ns
*
Polo^WT::GFP
Polo^T182D::GFP
Polo^T182A::GFP
Polo^K54M::GFP
polo
Polo^WT::GFP;polo
Polo^T182D::GFP;polo
Polo^T182A::GFP;polo
Polo^K54M::GFP;polo
E
Time in mitosis (min)
30
0
Control
mad2^P
Polo^T182D::GFP
Polo^T182D::GFP;mad2^P
polo,mad2^P
Polo^T182D::GFP; polo,mad2^P

Figure 2

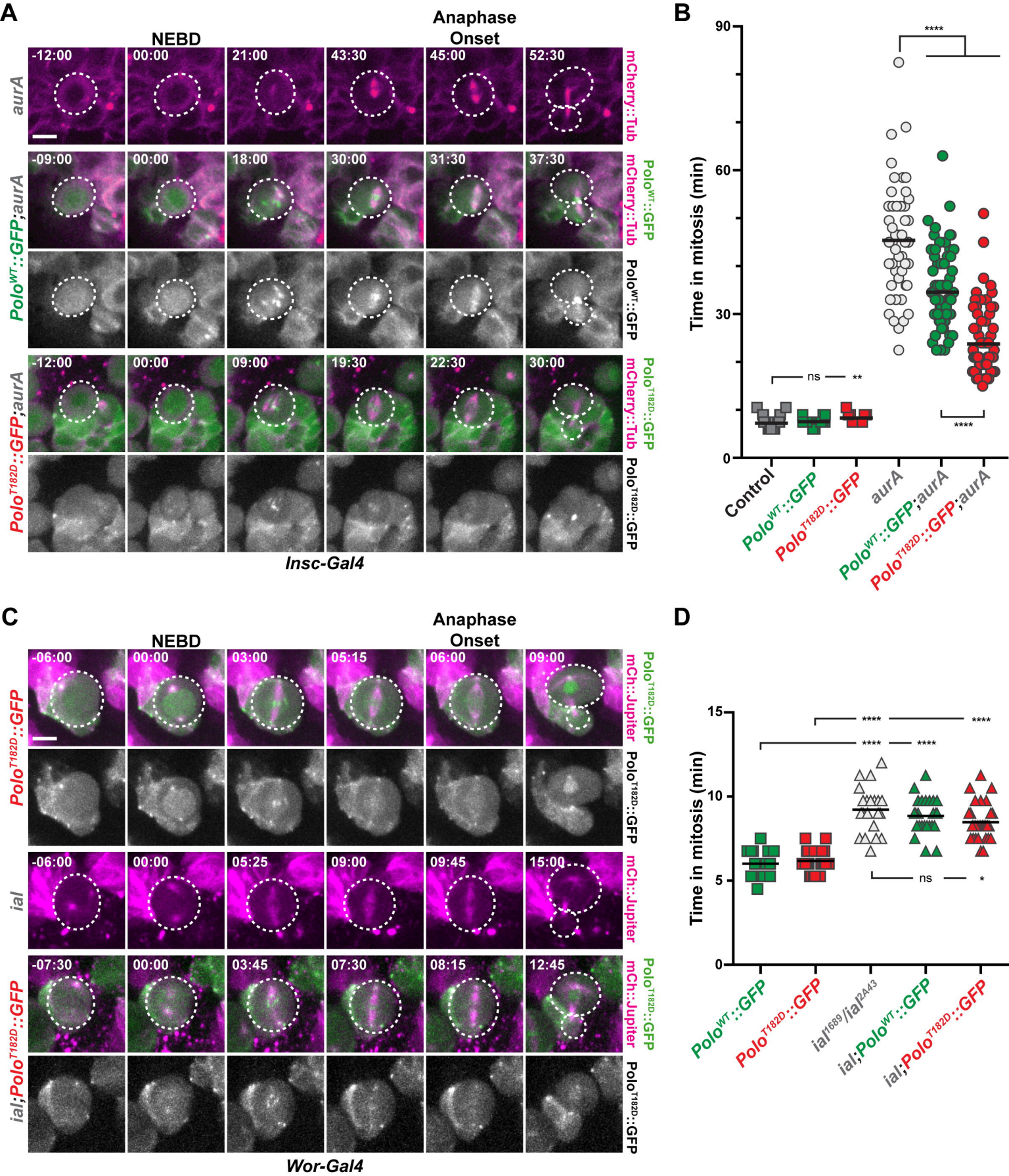
A
NEBD
Anaphase Onset
-12:00
00:00
21:00
43:30
45:00
52:30
aurA
mCherry::Tub
-09:00
00:00
18:00
30:00
31:30
37:30
PoloWT::GFP;aurA
mCherry::Tub
PoloWT::GFP
-12:00
00:00
09:00
19:30
22:30
30:00
PoloT182D::GFP;aurA
mCherry::Tub
PoloT182D::GFP
Insc-Gal4
B
Time in mitosis (min)
90
60
30
0
****
ns
**
****
Control
PoloWT::GFP
PoloT182D::GFP
aurA
PoloWT::GFP;aurA
PoloT182D::GFP;aurA
C
NEBD
Anaphase Onset
-06:00
00:00
03:00
05:15
06:00
09:00
PoloT182D::GFP
mCh::Jupiter
PoloT182D::GFP
-06:00
00:00
05:25
09:00
09:45
15:00
ial
mCh::Jupiter
-07:30
00:00
03:45
07:30
08:15
12:45
ial;PoloT182D::GFP
mCh::Jupiter
PoloT182D::GFP
Wor-Gal4
D
Time in mitosis (min)
15
10
5
0
****
****
****
****
ns
*
PoloWT::GFP
PoloT182D::GFP
ial1689/ial2A43
ial;PoloWT::GFP
ial;PoloT182D::GFP

Figure 3

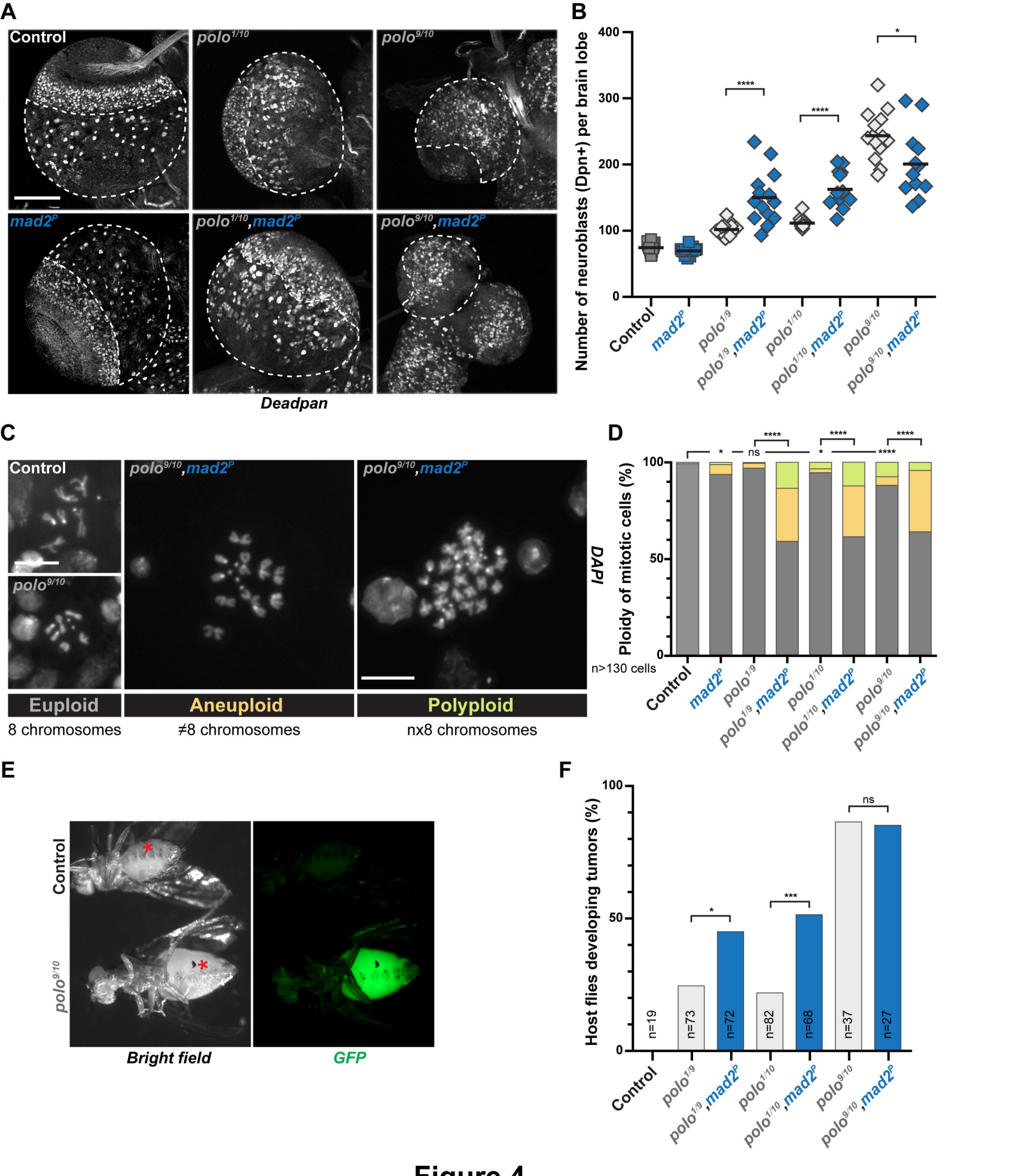
A
Control
polo1/10
polo9/10
mad2P
polo1/10,mad2P
polo9/10,mad2P
Deadpan
B
Number of neuroblasts (Dpn+) per brain lobe
400
300
200
100
0
****
****
*
Control
mad2P
polo1/9
polo1/9,mad2P
polo1/10
polo1/10,mad2P
polo9/10
polo9/10,mad2P
C
Control
polo9/10
polo9/10,mad2P
polo9/10,mad2P
DAPI
Euploid
Aneuploid
Polyploid
8 chromosomes
≠8 chromosomes
nx8 chromosomes
D
Ploidy of mitotic cells (%)
100
50
0
n>130 cells
*
ns
****
*
****
****
****
Control
mad2P
polo1/9
polo1/9,mad2P
polo1/10
polo1/10,mad2P
polo9/10
polo9/10,mad2P
E
Control
polo9/10
Bright field
GFP
F
Host flies developing tumors (%)
100
50
0
n=19
n=73
n=72
n=82
n=68
n=37
n=27
*
***
ns
Control
polo1/9
polo1/9,mad2P
polo1/10
polo1/10,mad2P
polo9/10
polo9/10,mad2P

Figure 4

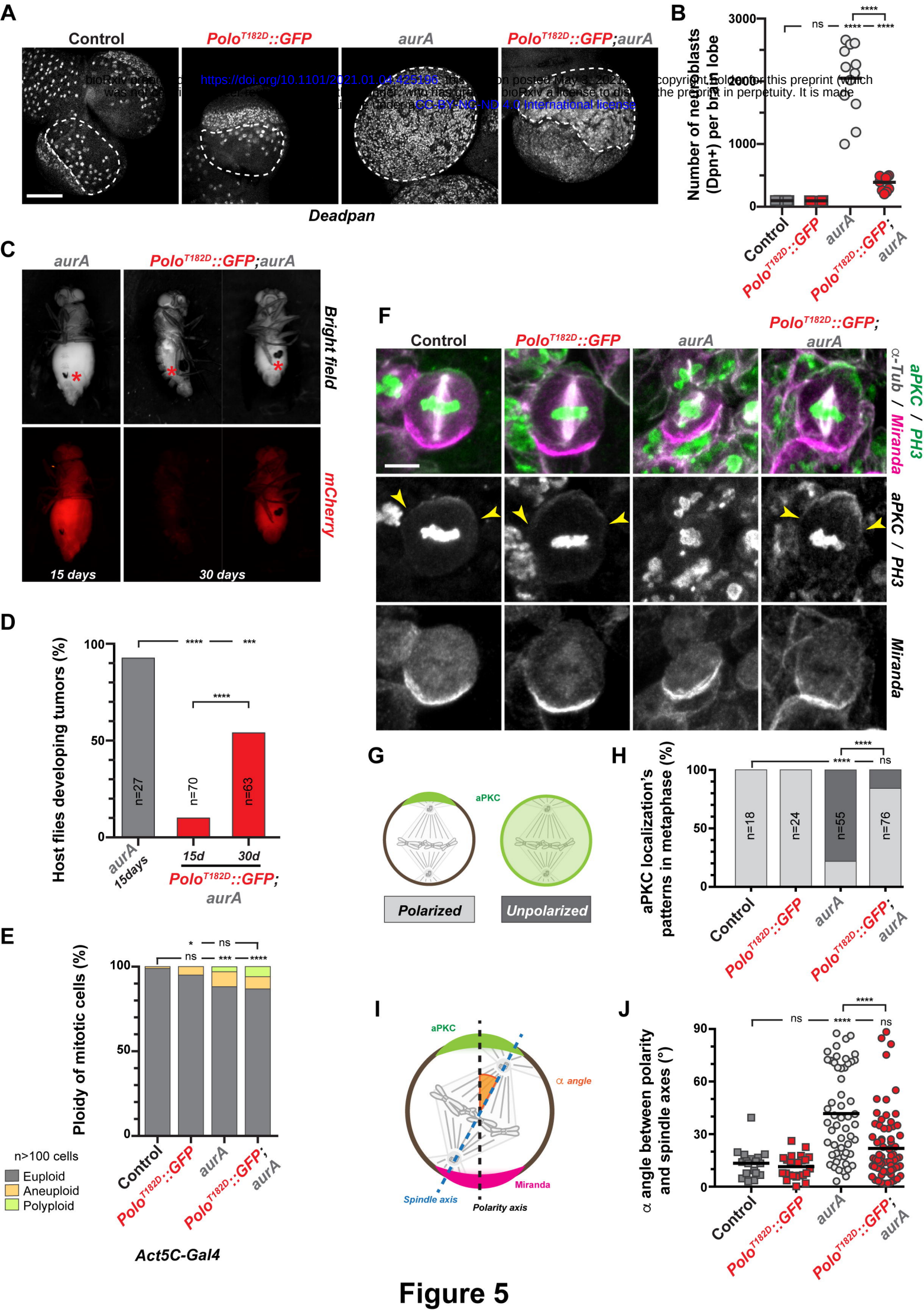

Figure 5